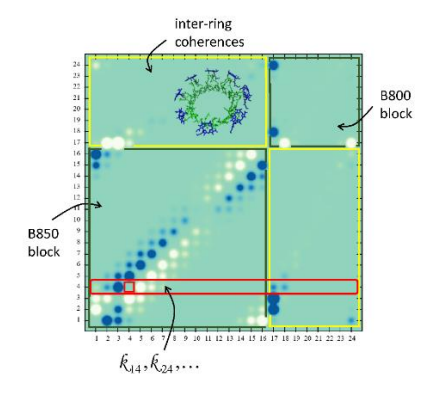
Coherence Maps and Flow of Excitation Energy in the Bacterial Light Harvesting Complex 2

Reshmi Dani¹, Sohang Kundu¹ and Nancy Makri^{*1,2,3}

Abstract

We present and analyze coherence maps [*J. Phys. Chem.* B **126**, 9361-9375] to investigate the quantum coherences that are created, sustained and damped by vibrational modes during the transfer of excitation energy from the B800 (outer) to the B850 (inner) ring of the light harvesting complex 2 (LH2) of purple bacteria with a variety of initial conditions. The reduced density matrix of the 24-pigment complex, where the ground and excited electronic states of each bacteriochlorophyll are explicitly coupled to 50 intramolecular vibrations at room temperature, is obtained from fully quantum mechanical small matrix path integral (SMatPI) calculations. The coherence maps show a very rapid localization within the outer ring, accompanied by the formation of inter-ring quantum superpositions that evolve to a partial quantum delocalization at equilibrium, and quantify in state-to-state detail the flow of energy within the complex.



¹Department of Chemistry, University of Illinois, Urbana, Illinois 61801, USA

²Department of Physics, University of Illinois, Urbana, Illinois 61801, USA

³Illinois Quantum Information Science and Technology Center, University of Illinois, Urbana, Illinois 61801, USA

^{*} Email: nmakri@illinois.edu

The process of solar light harvesting by photosynthetic bacteria and plants¹⁻² continues to attract intense attention. At the center of experimental and theoretical efforts is the quest for deciphering the intricate pathways of energy transfer, in particular the role of quantum mechanics in this highly efficient process.³⁻⁷ Understanding the mechanistic details of light harvesting in natural photosynthetic systems can also inform the design of artificial structures for clean energy production and storage.⁸⁻⁹

The structural characterization of the highly symmetric light harvesting complex 2 (LH2) of purple bacteria, ¹⁰⁻¹² composed of tightly packed, strongly coupled pigments, ¹³ along with the observation of beats in two-dimensional spectroscopic signals, ¹⁴⁻¹⁶ ignited a long-standing debate regarding the role that quantum coherence might play in the efficiency of energy transfer. ¹⁷ Many experimental and theoretical studies ^{5-6,18-35} reached a variety of conclusions in this regard, attributing the oscillatory signals to electronic delocalization, vibronic quantum coherence, or vibrational effects. For decades, theoretical investigations have implemented a variety of approaches, while accurate simulations have been hindered by the inability to accurately treat the electronic-nuclear dynamics of these very large complexes.

Very recent advances in real-time path integral methods³⁶⁻⁴³ have enabled numerically exact, fully quantum mechanical calculations in systems with a fairly large number of electronic states and any number of intramolecular normal mode vibrations at zero or finite temperatures. Using these methods, we recently reported the detailed evolution of excited states in bacteriochlorophyll (BChl) aggregates, both within the B850 (inner) ring of the LH2 complex⁴⁴ as well as during the ring-to-ring transfer following photoexcitation of either a single peripheral pigment⁴⁵ or an exciton eigenstate of the B800 band.⁴⁶ These simulations were performed on the symmetric complex (without static disorder) described by the Frenkel exciton Hamiltonian⁴⁷ of the 24 excited BChl states, with 50 intramolecular normal mode vibrations that couple to the ground and excited electronic states of each BChl unit with Huang-Rhys factors from fluorescence line narrowing experiments.⁴⁸ The path integral results showed that while the stronger excitonic couplings in the tightly packed inner ring create the necessary thermodynamic drive for inward ring-to-ring energy transfer, the efficient inter-ring energy transfer pathway in the LH2 complex is kinetically enabled by nuclear fluctuations.⁴⁵

In this Letter we supplement our earlier findings with an analysis of the excitation energy transfer (EET) pathways based on coherence maps.⁴⁹ A coherence map (C-map) is a pair of snapshots that depict the real and imaginary parts of the system's reduced density matrix (RDM) $\tilde{\rho}(t)$ on the square grid of system states at a particular time t. The temporal evolution of the C-map offers a very effective visualization of a dynamical process in a multistate system because the magnitude and distribution of real and imaginary components encodes a wealth of dynamical information:⁴⁹ A completely incoherent, stationary ensemble has a real, diagonal RDM in the site representation. Off-diagonal elements indicate contributions from coherent quantum superpositions of states. If one or more imaginary components are nonzero, such superpositions are forming or undergoing coherent evolution. At equilibrium all imaginary components vanish and the spread of the real-valued C-map indicates the quantum delocalization of the RDM. Further, when the coupling to the environment is diagonal in the basis of system states, as in the case of the Frenkel-type exciton-vibration Hamiltonian, ⁵⁰⁻⁵¹ the time evolution of site populations is completely determined by the imaginary components of off-diagonal RDM elements, weighted by state-to-state electronic couplings H_{jk}^{e} according to the relations of the relations to the relations of the relat

$$\frac{d}{dt}P_k(t) = \sum_{i=1}^n k_{jk}(t) \tag{1.1}$$

where $P_k(t) = \tilde{\rho}_{kk}(t)$, and n is the number of electronic states and

$$\mathcal{K}_{jk}(t) = \frac{2}{\hbar} H_{jk}^{e} \operatorname{Im} \tilde{\rho}_{jk}(t)$$
 (1.2)

is the contribution from site j to the instantaneous rate of population change of site k. Thus, the imaginary components in the C-map, weighted by the corresponding system (electronic) coupling elements, can be interpreted as instantaneous state-to-state rates (SSR).⁵² (Note that "instantaneous rate" refers to the time derivative of the population under consideration as given in Eq. (1.1), and does not imply that the electronic system obeys rate kinetics.) These quantities reveal which states contribute to the growth of a particular state population and which are responsible for its depletion.

The Hamiltonian for the n = 24-pigment LH2 system of *Rhodospirillum molischianum* has the Frenkel exciton form,⁴⁷ augmented with harmonic terms that represent molecular vibrations as well as a dissipative background arising from the protein and solvent environment and is given by⁵³

$$\hat{H} = \hat{H}^{e} + \hat{H}^{ev} \tag{1.3}$$

The first term,

$$\hat{H}^{c} = \sum_{k=1}^{n} \mathscr{C}_{k} |k\rangle\langle k| + \sum_{k=1}^{n} \sum_{k'\neq k}^{n} J_{kk'} |k\rangle\langle k'| = \sum_{i=0}^{n} E_{i} |\varphi_{i}\rangle\langle\varphi_{i}|, \qquad (1.4)$$

is the electronic Hamiltonian, where $|k\rangle$ are singly excited states with energies

$$\mathscr{C}_{k} = \varepsilon_{k}^{e} + \sum_{k' \neq k}^{n} \varepsilon_{k'}^{g} \tag{1.5}$$

and $J_{kk'}$ is the electronic coupling between pigments k,k', with values obtained using the collective electronic oscillators (CEO) method combined with Zerner's intermediate neglect of differential overlap with parameters for spectroscopic properties (ZINDO/S) electronic structure calculations reported in ¹³. All pigments of the outer ring, as well as the odd-numbered pigments of the inner ring, have identical values of \mathcal{C}_k , while the even-numbered pigments have site energies that are lower by $84 \, \mathrm{cm}^{-1}$. ¹³ More recent ZINDO/S-CIS calculations (with the additional configuration interaction singles treatment⁵⁴) obtained somewhat smaller coupling values between neighboring pigments but did not report values for more distant interactions. ⁵⁵ In Eq. (1.4) we also express the electronic Hamiltonian in terms of its eigenstates φ_i and eigenvalues E_i . The second term in Eq. (1.3) is the electron-vibration coupling,

$$\hat{H}^{\text{ev}} = \sum_{k=1}^{n} \left(\hat{h}_{k}^{\text{e}} + \sum_{k' \neq k}^{n} \hat{h}_{k'}^{\text{g}} \right) |k\rangle\langle k|$$
(1.6)

where

$$\hat{h}_{k}^{g} = \sum_{i=1}^{v_{k}} \left(\frac{\hat{p}_{ik}^{2}}{2m} + \frac{1}{2} m \omega_{ik}^{2} \hat{q}_{ik}^{2} \right) \quad \text{and} \quad \hat{h}_{k}^{e} = \sum_{i=1}^{v_{k}} \left[\frac{\hat{p}_{ik}^{2}}{2m} + \frac{1}{2} m \omega_{ik}^{2} \left(\hat{q}_{ik} - \frac{c_{ik}}{m \omega_{ik}^{2}} \right)^{2} \right]$$
(1.7)

are the ground and excited Hamiltonians for the vibrational and background degrees of freedom of each pigment. The coupling coefficients of the intramolecular vibrations are obtained from highly accurate Huang-Rhys factors determined based on fluorescence anisotropy experiments⁴⁸ and an additional low-frequency Ohmic bath, qualitatively similar to those determined through earlier work on light harvesting complexes^{24,56-58} is added⁴⁶ to model the dissipative effects of the biomolecular medium. The 16 BChl molecules of the inner ring are labeled as k = 1, ..., 16, while those of the outer ring are labeled k = 17, ..., 24. The total spectral density is shown in Figure 1, along with the structure of the two-ring complex, its numbering, the electronic coupling parameters and the exciton eigenvalues.

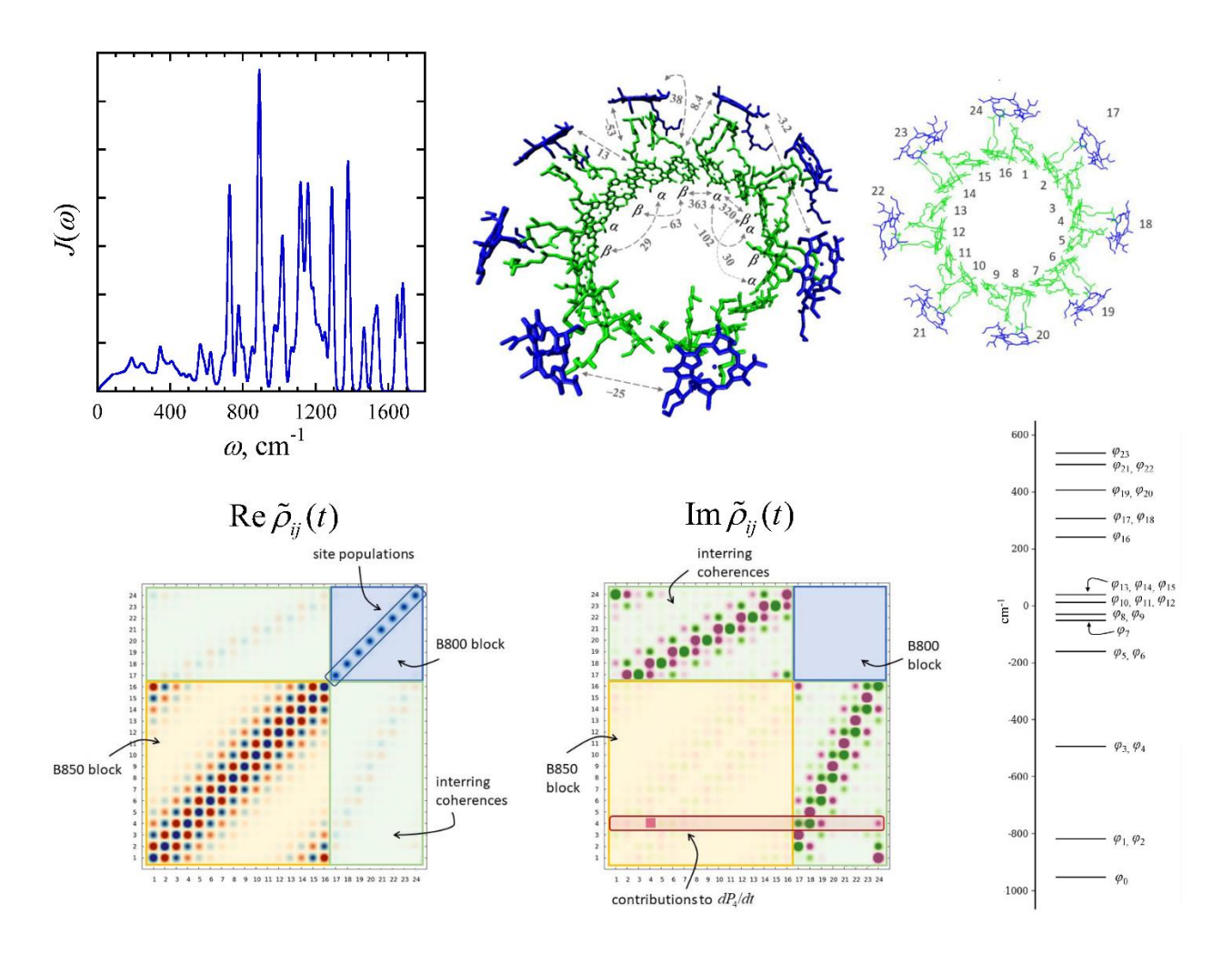


Fig. 1. Top: the spectral density and the structure of two-ring LH2 complex, showing electronic couplings and the site numbering. B800 pigments are in blue while B850 chromophores are shown in green. The structures are drawn using the Visual Molecular Dynamics software. ⁵⁹ Bottom: components of the LH2 C-maps and eigenvalues of the electronic Hamiltonian.

The basic structure of a C-map for the LH2 complex is also illustrated in Fig. 1. A pair of C-map images display the real and imaginary parts of the RDM on the 24×24 grid of excited BChl states. The 16×16 and 8×8 square blocks contain coherences within the B850 and B800 rings, respectively, while the two 16×8 and 8×16 rectangular blocks involve inter-ring coherences. The filling of these rectangular blocks indicates the formation of quantum superpositions between the two rings, and according to Eq. (1.2) the presence of nonzero imaginary components is a necessary condition for ring-to-ring energy transfer at the given time. The cyclic topology of each ring gives rise to the coherences in the corners of each block located opposite to the main diagonal.

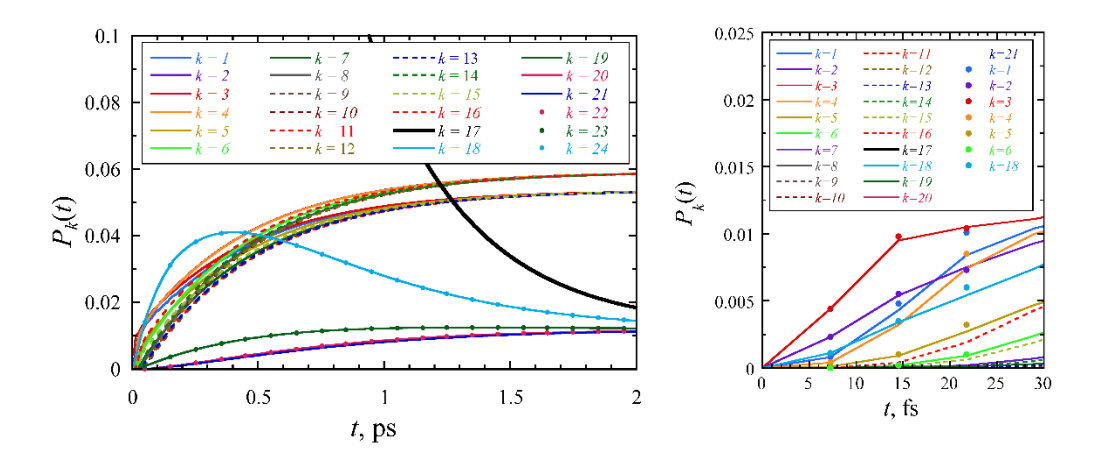


Fig. 2. Time evolution of site populations of the LH2 complex at room temperature following excitation of BChl 17. Left (data from Ref. ⁴⁵): Population dynamics over 2 ps. For visual clarity, the population axis is cropped at 0.1. The thick black line shows the population of the initially excited pigment. Right: Early time dynamics. In this panel markers show results obtained with only the discrete intramolecular vibrational modes included in the Hamiltonian, while lines show populations with the total spectral density, which includes a low-frequency background component.

Figure 2 shows the dynamics of excitation energy transfer at room temperature following excitation of a single monomer, BChl 17. The left panel shows results obtained in our recent calculations⁴⁵ using the fully quantum mechanical small matrix path integral (SMatPI) method,⁴¹⁻⁴³ which found that the portion of excitation energy transferred to the inner ring in the absence of exciton-vibration coupling is less than 15%. The time scale of ring-to-ring energy transfer obtained from these numerically exact calculations is in good agreement with experimental results,⁶⁰ suggesting that the parameters of the exciton Hamiltonian¹³ are sufficiently accurate for the EET dynamics. While the low-frequency background included in the spectral density is responsible for irreversible transfer and equilibration, the early EET steps, mediated by the quantum superpositions observed in the coherence maps we present, are governed by the high-frequency discrete intramolecular vibrations. This expectation is confirmed by the short-time path integral results shown in the right panel of Fig. 2, obtained with a spectral density that does not include the broad background component.

SMatPI results for the electronic eigenstate populations following excitation of φ_7 and of φ_{13} were reported in Ref. ⁴⁶. The first of these electronic eigenstates, composed primarily of outer ring excitations, is the lowest of the B800 electronic eigenstates, while φ_{13} lies well within the B800 band, yet has a mixed

character with 78% of the density on the inner ring. In both cases a very rapid initial relaxation within approximately 70 fs was observed. In the case of φ_7 initial excitation, the rapid decay is followed by a slow process that leads to population of low-lying eigenstates, while in the case of the mixed character state the dynamics is much faster and the populations reach near-equilibrium values within the initial ~70 fs relaxation.

Figures 3-5 show selected snapshots of the coherence maps in the site (excited pigment) representation for these three initial conditions that correspond to a single chromophore of the outer ring and the two electronic eigenstates of the B800 band discussed in the previous paragraph. For visual clarity, the range of the color map is adjusted separately for the real and imaginary components of each initial condition. The complete sequence of frames is given in the Supplementary Information. In addition to the C-map, we show the instantaneous SSR maps, whose elements are given by Eq. (1.2). The sum of the k^{th} entire row of the SSR map determines the overall time derivative of the population P_k at the given time.

(i) Monomer excitation

We first consider a monomer initial condition with the initial excitation confined to BChl 17 on the outer ring. Figure 3 shows the C-maps at approximately 22, 51 and 700 fs. Coherences develop extremely rapidly (within <10 fs) on the neighboring peripheral units 18 and 24, as well as on nearby pigments of the inner ring, primarily monomers 1-4. The imaginary components of these RDM elements, weighted by elements of the electronic Hamiltonian, determine the rate of population growth of the site in the given row. Even though $\text{Im } \tilde{\rho}_{i,17}$ changes sign multiple times within this row, the sign of the electronic matrix elements also changes, such that all coupled pigments contribute to the depletion of BChl 17. This is clearly seen in the instantaneous SSR maps shown in the right column of Fig. 3, where it is seen that all BChl states in row 17 make either a negative or zero contribution to the instantaneous rate. Further, some states that have large imaginary coherences with BChl 17, such as monomers 16 and 15, do not contribute to the SSR because their electronic coupling elements are equal to zero. As seen in the real part of the C-map, excitation is building on pigments 1-4 at these early times (and less rapidly to 18 and 24, as these peripheral units have weaker couplings to BChl 17 and thus a slower population growth) but no population growth to sites 15 and 16 is observed at this time. The flow of excitation energy within the inner ring is clearly seen from the SSR map. Energy flows faster from BChl 17 to the excited state of monomer 3 than to BChl 2 (because of electronic coupling strengths). Further, excitation energy leaks out of BChl 3 to all its neighboring pigments, while states 2 and 4 receive energy from state 3 and pass on the energy to their other neighbors.

These early superpositions give rise to a whole series of secondary coherences between the B850 pigments that are being populated and their neighbors. The strongest couplings between inner ring pigments lead to the rapid spreading of the excitation through these secondary coherences. This spreading can be seen even in the early C-map at 22 fs, and by 100 fs grows to a weak superposition that involves the majority of inner ring pigments. No such superposition is formed on the outer ring, except for the small population of nearby pigments. The absence of such superpositions from the perfectly symmetric B800 ring is the consequence of vibrational motion, which is a relatively more effective source of decoherence on the weakly coupled peripheral pigments in comparison to the tightly bound inner ring.⁴⁵

As time progresses, the imaginary parts of intra-B850 RDM elements gradually begin to fade, while the corresponding real components stabilize. Strong inter-ring coherences remain within the row and column that contain BChl 17, whose population decays over a ~1 ps time scale. When equilibrium is

reached, the real part of the C-map is very similar to the \sim 700 fs snapshot seen in Fig. 3, and all imaginary components have decayed to zero. The C-map shown in the last panel of Fig. 3 conveys a clear picture of the equilibrium distribution, which involves a quantum superposition of excited pigments on the inner ring. The alternating signs of RDM elements are a manifestation of the positive couplings between adjacent pigments of the B850 ring. The C-map is dominated by a diagonal band whose width spans 3-4 units in either direction with respect to the main diagonal that contains the BChl populations. Thus, the equilibrium coherence span revealed from the C-map is in excellent agreement with that obtained in earlier work. $^{18,22,44,61-62}$

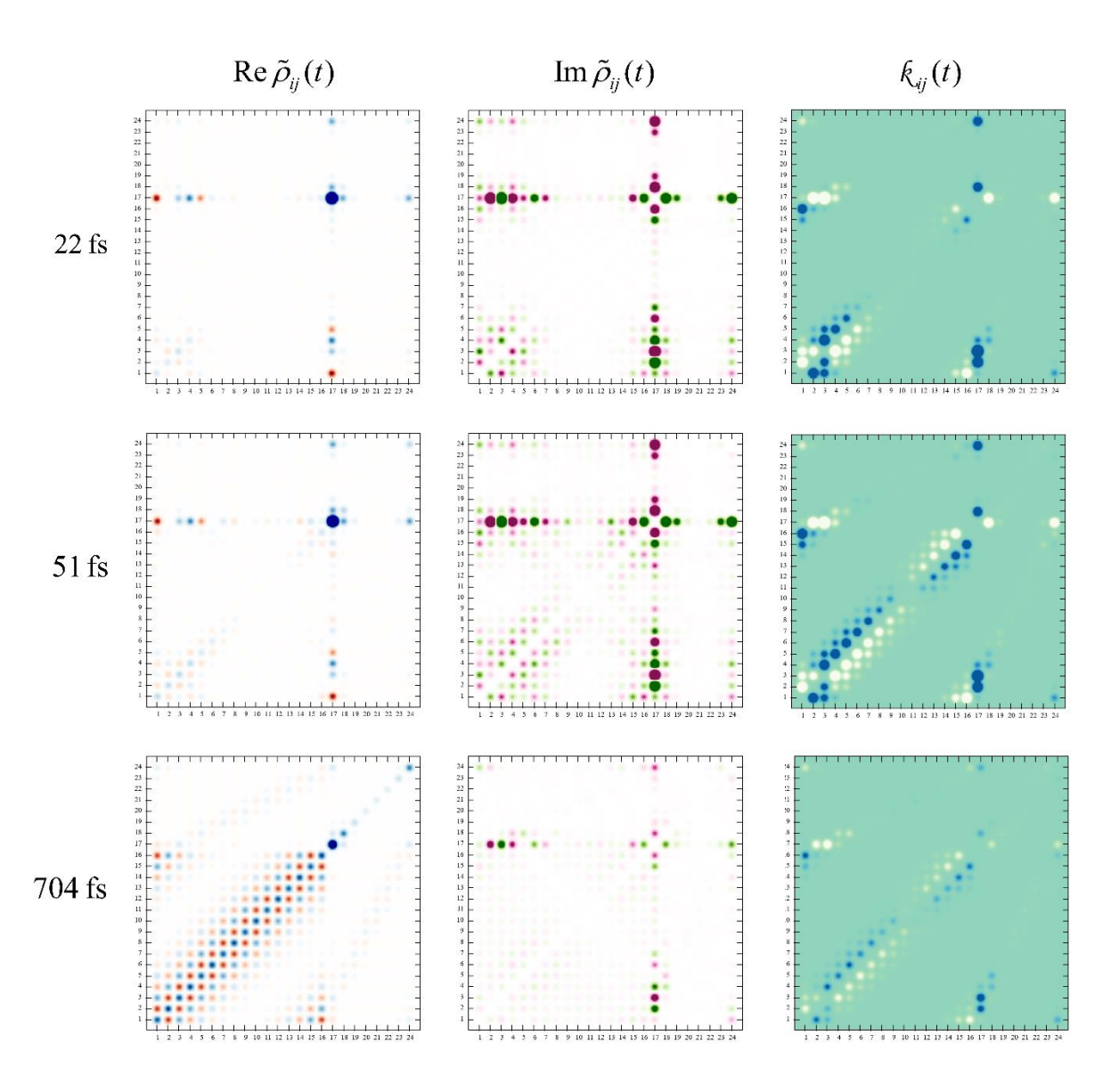


Fig. 3. Coherence and instantaneous SSR maps with the initial excitation placed on BChl 17. The left and middle columns show the real and imaginary parts of the RDM elements. Blue and green correspond to positive regions, while red and magenta correspond to negative regions. The right column shows the SSR map, Eq. (1.2). Blue and white correspond to positive and negative rates, respectively.

(ii) Excitation of a B800 eigenstate

Next, we examine in Figure 4 the EET dynamics following excitation of electronic eigenstate φ_7 . This is the lowest-lying state of the B800 band, with contributions mainly from peripheral pigments. The site composition of this eigenstate can be inferred from the first panel of Fig. 4. As the ground state of the outer ring, this eigenstate is fully delocalized, and since the electronic coupling between adjacent outer ring chromophores has a negative value, all BChl states contribute with coefficients of the same sign. One can observe weak superpositions of alternating signs involving inner ring units, the result of small components in the electronic eigenstates.

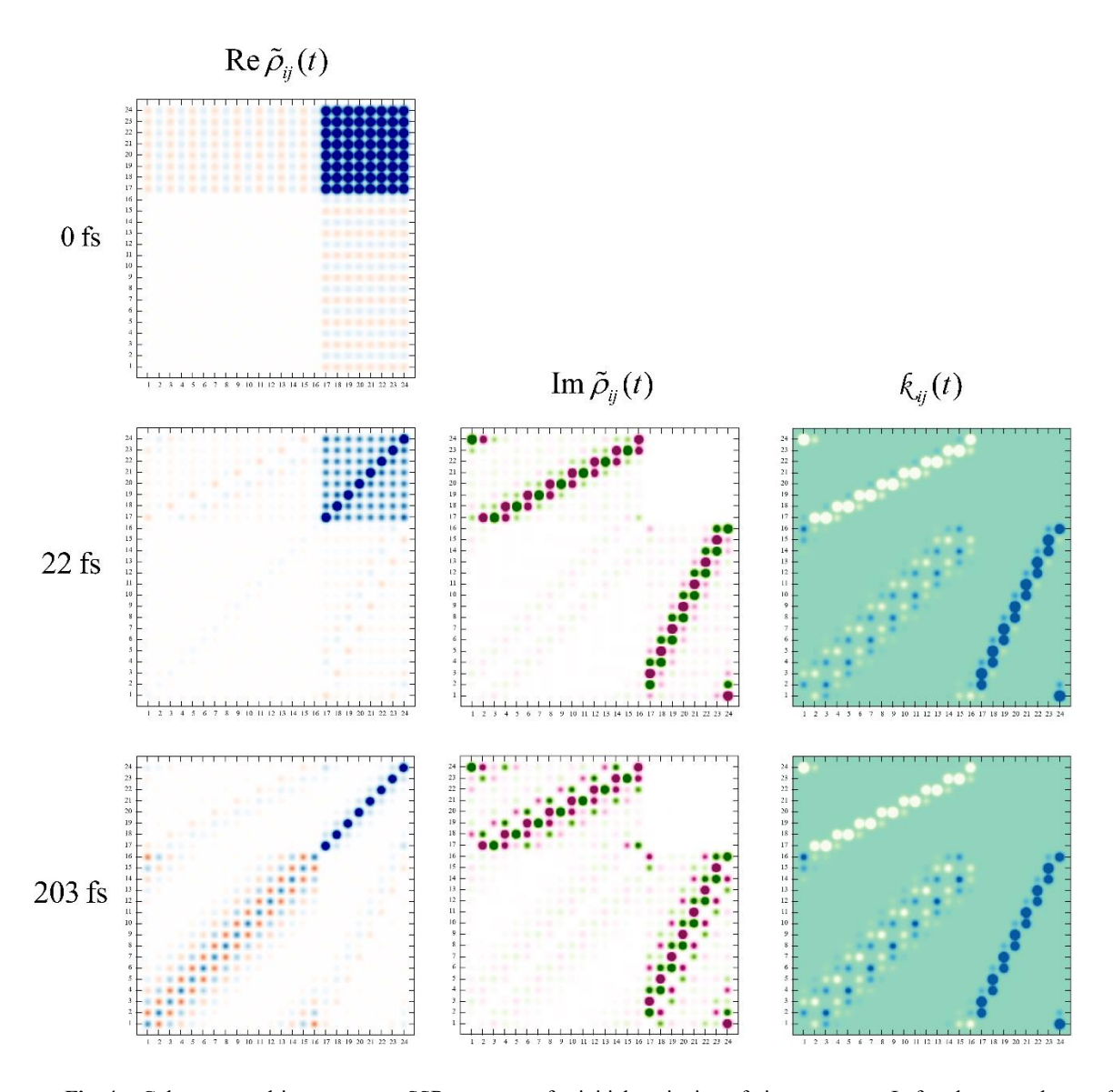


Fig. 4. Coherence and instantaneous SSR rate maps for initial excitation of eigenstate φ_7 . Left column: real part of RDM elements. Right: imaginary part of RDM elements. The top right panel shows the structure of the complex along with electronic coupling values. Blue and green correspond to positive regions, while red and magenta correspond to negative regions. The right column shows the SSR map, Eq. (1.2). Blue and white correspond to positive and negative rates, respectively.

The early evolution of the C-map shown in Fig. 4 is dominated by two features: First, imaginary coherences develop between each populated B800 unit and its neighboring pigments, in analogy to the pattern observed in Fig. 3. Since all BChls of the outer ring initially have identical populations equal to $P_k(0) = 1/8$, off-diagonal RDM elements have reduced values and form bands with respect to the diagonals of the two rectangles, which contain inter-ring coherences that show a nontrivial variation of signs. Note that despite the initial condition being a quantum superposition over the B800 block, no imaginary coherences emerge within it, as the populations of all peripheral sites remain equal to each other at all times. Second, as seen in the 22 fs snapshot shown in the middle panels, real-valued off-diagonal components within the outer ring, which initially had equal magnitude, are seen to decay very rapidly, such that at 70 fs the peripheral complex portion of the C-map is entirely localized about the diagonal. Thus, all coherence dies out very rapidly within the B800 ring, giving rise to a mostly incoherent ensemble of excited pigments. A fully incoherent RDM implies equal participation from all eigenstates of the system. Indeed, all eigenstates of the B800 ring are populated with nearly comparable probabilities within approximately 70 fs following excitation of eigenstate φ_7 . The very rapid intra-B800 localization is primarily the consequence of the high-frequency intra-chromophore vibrations.

The subsequent dynamics consists of B800-to-B850 energy transfer following the mechanism discussed in (i), mediated by the imaginary coherences shown in the C-map, which persist for approximately 1 ps. Eventually the two-ring complex equilibrates, giving rise to a C-map that is identical to that attained at long times with other initial conditions.

In contrast to the dynamics following excitation of a monomer, energy flows inward from all outer ring pigments in the present case. However, the asymmetric placement of the B800 pigments with respect to those of the inner ring and the dimerization within the B850 complex lead to nontrivial energy flow patterns. The SSR map shows that all odd-numbered B850 pigments give energy to their immediate neighbors. However, for odd k, BChl k gives energy to pigment k-2 as well, but receives energy from pigment k+2, in spite of identical electronic couplings.

(iii) Excitation of mixed-character eigenstate

Last, we present in Figure 5 the evolution of the C-map following excitation of eigenstate φ_{13} , which has a mixed B800-B850 character with 78% of the density located on the inner ring. As seen from the t=0 panel, this eigenstate has contributions from all excited pigments of the LH2 complex. Its composition in terms of peripheral pigments suggests that its outer ring component consists of the highest energy electronic eigenstate of the isolated B800 ring. The inner-ring component of φ_{13} correlates with an excited state of the isolated B850 ring.

The early evolution of this eigenstate shares some of the characteristics identified in the relaxation of eigenstate φ_7 , as well as distinct features. First, the B800 block undergoes again a rapid localization (decay of off-diagonal elements) within the outer ring within 70 fs, which results in the small population of other B800 eigenstates. However, in contrast to the C-map from the excited eigenstate φ_7 , where a band of B800-B850 superpositions was observed, in the present case large imaginary coherences develop that are spread over the entire inter-ring blocks. These imaginary components indicate a rapid population transfer from the B800 pigments to the inner ring, mediated by the combination of inner- and outer-ring excitations in the chosen eigenstate, and quickly localize to a band while beginning to fade, as equilibration occurs much faster with this initial condition. In fact, the 22 fs SSR map shows that intra-B850 population transfer

is already dominant at this early time, in contrast to the trends observed with the previous initial conditions where inter-ring transfer is the dominant process until much later times.

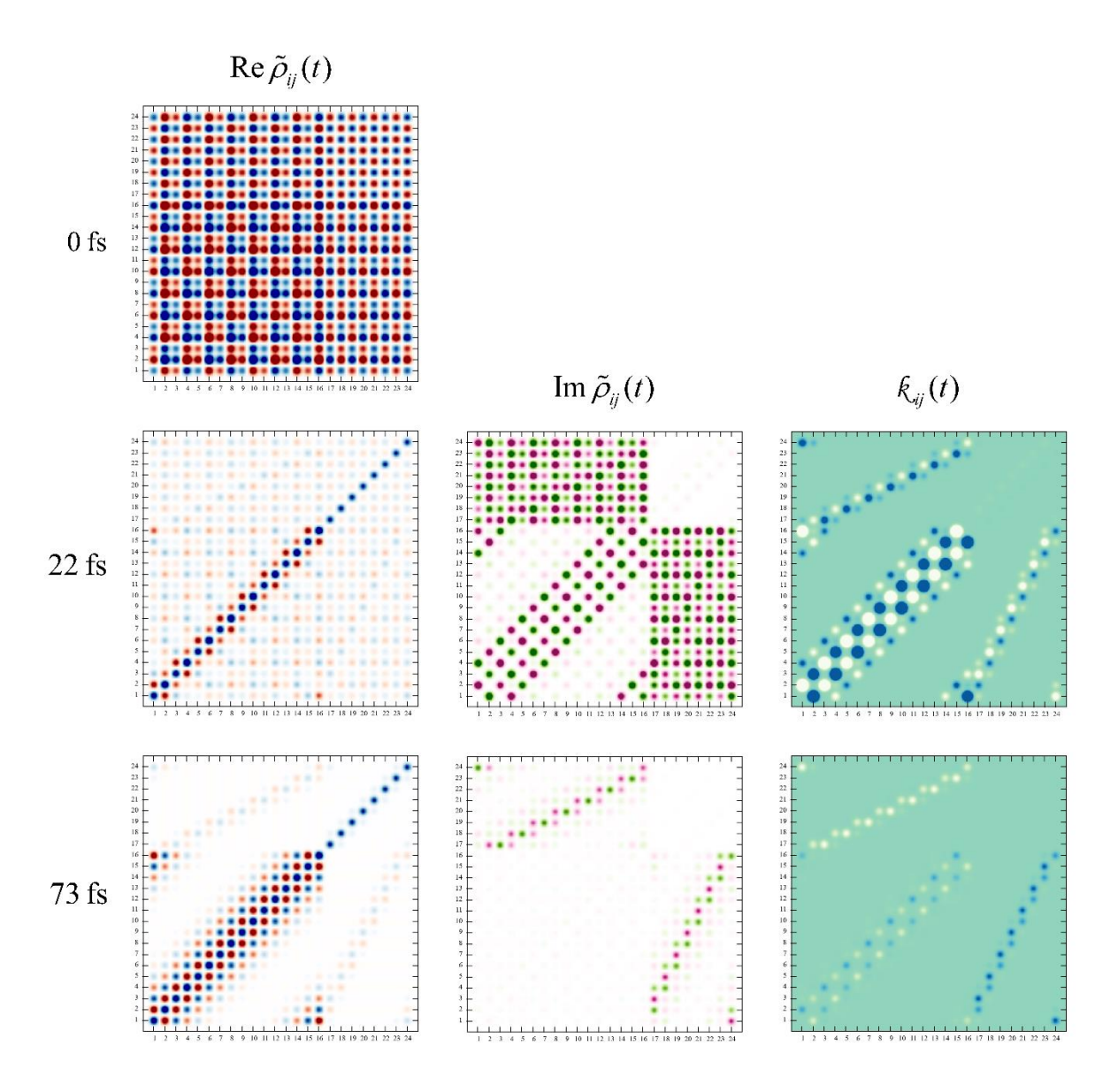


Fig. 5. Coherence and instantaneous state-to-state rate maps for initial excitation of eigenstate φ_{13} . Left column: real part of RDM elements. Right: imaginary part of RDM elements. The top right panel shows the structure of the complex along with electronic coupling values. Blue and green correspond to positive regions, while red and magenta correspond to negative regions. The right column shows the SSR map, Eq. (1.2). Blue and white correspond to positive and negative rates, respectively.

The quantum superpositions within the B850 ring show interesting patterns that are different from those observed in the other C-maps. First, the real part of the initially fully delocalized C-map appears considerably localized at 22 fs but subsequently spreads out, approaching the equilibrium band. The

transient localization occurs because the real part of many coherences changes sign early on, as the ring begins to settle to its equilibrium distribution, temporarily attaining near-zero values. Second, Im $\tilde{\rho}_{ij} \neq 0$ only if i+j is an odd index. The consequence of this feature is the absence of energy flow between second nearest neighbor (k to $k \pm 2$) pigments of the inner ring, in spite of strong couplings. Further, the SSR map shows that the flow of energy within the inner ring has the opposite direction within each BChl dimer, with odd-numbered units receiving energy from both of their immediate neighbors.

In conclusion, the analysis of C-maps offers a wealth of dynamical information regarding the flow of energy within the LH2 complex, and it is not possible to summarize all the features of the EET pathways that were vividly borne out of these visualizations of RDM evolution. C-maps show the composition and extent of quantum superpositions and their fates on the way to equilibrium. A very rapid localization of initially excited B800 eigenstates and the creation of inter-ring coherences that drive population transfer, mediated by discrete vibrational modes, are borne out very clearly through the C-map visualization. The formation at long times of a partially delocalized RDM band over the B850 block conveys the nature of the equilibrium ensemble. The imaginary component of the C-map and the closely related instantaneous SSR map reveal the pathways of energy flow between and within the two rings with unprecedented detail and clarity.

The real-time path integral results on which the C-maps were based were obtained for the symmetric two-ring complex where the intramolecular vibrational modes of each pigment were included through accurate Huang-Rhys factors obtained from fluorescence line narrowing data and low-frequency fluctuations associated with protein motion were modeled via a broad spectral density term. Static disorder can distort the symmetry of the complex. Given the large magnitude of electronic coupling terms between adjacent pigments, the induced asymmetry may lead to a partial (but not complete) localization of the exciton eigenstates. ^{19,63-65} It will be interesting to quantify the effect of static disorder on the energy transfer pathways of the LH2 complex by performing additional path integral simulations, along with a C-map analysis.

Supporting Information

Animation of the LH2 coherence maps.

Acknowledgements

This material is based upon work supported by the National Science Foundation under Award CHE-1955302. This research is part of the Delta research computing project, which is supported by the National Science Foundation (award OCI 2005572) and the State of Illinois. Delta is a joint effort of the University of Illinois at Urbana-Champaign and its National Center for Supercomputing Applications.

References

- (1) Pullerits, T.; Sundstrom, V., Photosynthetic light-harvesting pigment-protein complexes: Toward understanding how and why. *Acc. Chem. Res.* **1996**, *29*, 381-389.
- (2) Blankenship, R. E., *Molecular mechanisms of photosynthesis*. World Scientific: London, 2002.
- (3) Ishizaki, A.; Fleming, G. R., Quantum Coherence in Photosynthetic Light Harvesting. *Annual Review of Condensed Matter Physics* **2012**, *3* (1), 333-361.
- (4) Chenu, A.; Scholes, G. D., Coherence in Energy Transfer and Photosynthesis. *Annual Review of Physical Chemistry* **2015**, *66* (1), 69-96.
- (5) Mirkovic, T.; Ostroumov, E. E.; Anna, J. M.; van Grondelle, R.; Govindjee; Scholes, G. D., Light Absorption and Energy Transfer in the Antenna Complexes of Photosynthetic Organisms. *Chemical Reviews* **2017**, *117* (2), 249-293.
- (6) Cao, J.; Cogdell, R. J.; Coker, D. F.; Duan, H.-G.; Hauer, J.; Kleinekathöfer, U.; Jansen, T. L. C.; Mančal, T.; Miller, R. J. D.; Ogilvie, J. P.; Prokhorenko, V. I.; Renger, T.; Tan, H.-S.; Tempelaar, R.; Thorwart, M.; Thyrhaug, E.; Westenhoff, S.; Zigmantas, D., Quantum biology revisited. *Science Advances* **2020**, *6* (14), eaaz4888.
- (7) Kundu, S.; Makri, N., Intramolecular vibrations in excitation energy transfer: Insights from real-time path integral calculations. *Annual Review of Physical Chemistry* **2022**, *73* (1), 349-375.
- (8) Balzani, V.; Credi, A.; Venturi, M., Photochemical Conversion of Solar Energy. *ChemSusChem* **2008**, *I* (1-2), 26-58.
- (9) Barber, J., Photosynthetic energy conversion: natural and artificial. *Chemical Society Reviews* **2009**, *38* (1), 185-196.
- (10) McDermott, G.; Prince, S.; Freer, A.; Hawthornthwaite-Lawless, A.; Papiz, M.; Cogdell, R.; Isaacs, N., Crystal structure of an integral membrane light-harvesting complex from photosynthetic bacteria. *Nature* **1995**, *374*, 517.
- (11) Hu, X.; Xu, D.; Hamer, K.; Schulten, K.; Koepke, J.; Michel, H., Predicting the structure of the light harvesting complex II of rhodospirillum molischianum. *Protein Science* **1995**, *4*, 1670-1682.
- (12) Koepke, J.; Hu, X.; Muenke, C.; Schulten, K.; Michel, H., The crystal structure of the light harvesting complex II (B800-B850) from Rhodospirillum molischianum. *Structures* **1996**, *4*, 581-597.
- (13) Tretiak, S.; Middleton, C.; Chernyak, V.; Mukamel, S., Exciton Hamiltonian for the bacteriochlorophyll system in the LH2 antenna complex of purple bacteria. *J. Phys. Chem. B* **2000**, *104*, 4519-4528.
- (14) Calhoun, T. R.; Ginsberg, N. S.; Schlau-Cohen, G. S.; Cheng, Y.-C.; Ballottari, M.; Bassi, R.; Fleming, G. R., Quantum Coherence Enabled Determination of the Energy Landscape in Light-Harvesting Complex II. *The Journal of Physical Chemistry B* **2009**, *113* (51), 16291-16295.
- (15) Harel, E.; Engel, G. S., Quantum coherence spectroscopy reveals complex dynamics in bacterial light-harvesting complex 2 (LH2). *Proceedings of the National Academy of Sciences* **2012**, *109* (3), 706-711.
- (16) Kim, J.; Nguyen-Phan, T. C.; Gardiner, A. T.; Cogdell, R. J.; Scholes, G. D.; Cho, M., Low-Frequency Vibronic Mixing Modulates the Excitation Energy Flow in Bacterial Light-Harvesting Complex II. *The Journal of Physical Chemistry Letters* **2021**, *12* (27), 6292-6298.
- (17) Hu, X.; Ritz, T.; Damjanovic, A.; Schulten, K., Pigment organization and transfer of electronic excitation in the photosynthetic unit of purple bacteria. *J. Phys. Chem.* **1997**, *101*, 3854-3871.
- (18) Meier, T.; Zhao, Y.; Chernyak, V.; Mukamel, S., Polarons, localization, and excitonic coherence in superradiance of biological antenna complexes. *J. Chem. Phys.* **1997**, *107*, 3876-3893.
- (19) Kühn, O.; Sundstrom, V., Pump-probe spectroscopy of dissipative energy transfer dynamics in photosynthetic antenna complexes: A density matrix approach. *J. Chem. Phys.* **1997**, *107*, 4154-4164.
- (20) Sundstrom, V.; Pullerits, T.; van Grondelle, R., Photosynthetic light harvesting: Reconciling dynamics and structure of purple bacterial LH2 reveals function of photosynthetic unit. *J. Phys. Chem. B* **1999**, *103*, 2327-2346.

- (21) Mukai, K.; Abe, S.; Sumi, H., Theory of Rapid Excitation-Energy Transfer from B800 to Optically-Forbidden Exciton States of B850 in the Antenna System LH2 of Photosynthetic Purple Bacteria. *The Journal of Physical Chemistry B* **1999**, *103* (29), 6096-6102.
- (22) Ray, J.; Makri, N., Short range coherence in the energy transfer of photosynthetic light harvesting systems. *J. Phys. Chem.* **1999**, *103*, 9417-9422.
- (23) Scholes, G. D.; Fleming, G. R., On the Mechanism of Light Harvesting in Photosynthetic Purple Bacteria: B800 to B850 Energy Transfer. *The Journal of Physical Chemistry B* **2000**, *104* (8), 1854-1868.
- (24) Adolphs, J.; Renger, T., How proteins trigger excitation energy transfer in the FMO complex of green sulfur bacteria. *Biophys J.* **2006**, *91*, 2778–2797.
- (25) Jang, S.; Newton, M. D.; Silbey, R. J., Multichromophoric Förster Resonance Energy Transfer from B800 to B850 in the Light Harvesting Complex 2: Evidence for Subtle Energetic Optimization by Purple Bacteria. *The Journal of Physical Chemistry B* **2007**, *111* (24), 6807-6814.
- (26) Ishizaki, A.; Fleming, G. R., Theoretical examination of quantum coherence in a photosynthetic system at physiological temperature. *Proceedings of the National Academy of Sciences* **2009**, *106* (41), 17255-17260.
- (27) Tao, G.; Miller, W. H., Semiclassical description of electronic excitation population transfer in a model photosynthetic system. *J. Phys. Chem. Lett.* **2010**, *1*, 891-894.
- (28) Collini, E.; Wong, C. Y.; Wilk, K. E.; Curmi, P. M. G.; Brumer, P.; Scholes, G. D., Coherently wired light-harvesting in photosynthetic marine algae at ambient temperature. *Nature* **2010**, *463*, 644.
- (29) Huo, P.; Coker, D. F., Iterative linearized density matrix propagation for modeling coherent excitation energy transfer in photosynthetic light harvesting. *J. Chem. Phys.* **2010**, *133*, 184108.
- (30) Abramavicius, D.; Mukamel, S., Quantum oscillatory exciton migration in photosynthetic reaction centers. *J. Chem. Phys.* **2010**, *133*, 064510.
- (31) Womick, J. M.; Moran, A. M., Vibronic enhancement of exciton sizes and energy transport in photosynthetic complexes. *J. Phys. Chem. B* **2011**, *115*, 1347–1356.
- (32) Tiwari, V.; Peters, W. K.; Jonas, D. M., Electronic resonance with anticorrelated pigment vibrations drives photosynthetic energy transfer outside the adiabatic framework. *Proc. Nat. Acad Sci. USA* **2013**, *110*, 1203-1208.
- (33) Duan, H.-G.; Stevens, A. L.; Nalbach, P.; Thorwart, M.; Prokhorenko, V. I.; Miller, R. J. D., Two-dimensional electronic spectroscopy of light-harvesting complex II at ambient temperature: A joint experimental and theoretical study. *The Journal of Physical Chemistry B* **2015**, *119* (36), 12017-12027.
- (34) Duan, H.-G.; Prokhorenko, V. I.; Cogdell, R. J.; Ashraf, K.; Stevens, A. L.; Thorwart, M.; Miller, R. J. D., Nature does not rely on long-lived electronic quantum coherence for photosynthetic energy transfer. *Proceedings of the National Academy of Sciences* **2017**, 201702261.
- (35) Kreisbeck, C.; Kramer, T.; Aspuru-Guzik, A., Scalable High-Performance Algorithm for the Simulation of Exciton Dynamics. Application to the Light-Harvesting Complex II in the Presence of Resonant Vibrational Modes. *Journal of Chemical Theory and Computation* **2014**, *10* (9), 4045-4054.
- (36) Makri, N., Modular path integral: Quantum dynamics via sequential necklace linking. *J. Chem. Phys.* **2018**, *148*, 101101.
- (37) Makri, N., Modular path integral methodology for real-time quantum dynamics. *J. Chem. Phys.* **2018**, *149*, 214108.
- (38) Kundu, S.; Makri, N., Modular path integral for discrete systems with non-diagonal couplings. *J. Chem. Phys.* **2019**, *151*, 074110.
- (39) Kundu, S.; Makri, N., Modular path integral for finite-temperature dynamics of extended systems with intramolecular vibrations. *J. Chem. Phys.* **2020**, *153*, 044124.
- (40) Kundu, S.; Makri, N., Efficient matrix factorisation of the modular path integral for extended systems. *Mol. Phys.* **2021**, *119*, e1797200.
- (41) Makri, N., Small matrix disentanglement of the path integral: overcoming the exponential tensor scaling with memory length. *J. Chem. Phys.* **2020**, *152*, 041104.
- (42) Makri, N., Small matrix path integral for system-bath dynamics. *J. Chem. Theory and Comput.* **2020**, *16*, 4038–4049.

- (43) Makri, N., Small matrix path integral with extended memory. *J. Chem. Theory and Comput.* **2021**, *17*, 1-6.
- (44) Kundu, S.; Makri, N., Real-time path integral simulation of exciton-vibration dynamics in light-harvesting bacteriochlorophyll aggregates. *J. Phys. Chem. Lett.* **2020**, *11*, 8783-8789.
- (45) Kundu, S.; Dani, R.; Makri, N., Tight inner ring architecture and quantum motion of nuclei enable efficient energy transfer in bacterial light harvesting. *Science Advances* **2022**, *8* (43), eadd0023.
- (46) Kundu, S.; Dani, R.; Makri, N., B800-to-B850 relaxation of excitation energy in bacterial light harvesting: All-state, all-mode path integral simulations. *J. Chem. Phys.* **2022**, *157*, 115101.
- (47) Frenkel, J., On the transformation of light into heat in solids. *Phys. Rev.* **1931**, *37*, 17.
- (48) Rätsep, M.; Cai, Z.-L.; Reimers, J. R.; Freiberg, A., Demonstration and interpretation of significant asymmetry in the low-resolution and high-resolution Qy fluorescence and absorption spectra of bacteriochlorophyll a. *J. Chem. Phys.* **2011**, *134*, 024506.
- (49) Dani, R.; Makri, N., Time-Evolving Quantum Superpositions in Open Systems and the Rich Content of Coherence Maps. *The Journal of Physical Chemistry B* **2022**, *126* (45), 9361-9375.
- (50) May, V.; Kuhn, O., Theory of charge and energy transfer in molecular systems. Wiley: 1999.
- (51) May, V.; Kühn, O., Charge and energy transfer dynamics in molecular systems. 3rd ed.; Wiley: 2011.
- (52) Dani, R.; Makri, N., Quantum State-to-State Rates for Multistate Processes from Coherences. *The Journal of Physical Chemistry Letters* **2022**, *13* (34), 8141-8149.
- (53) Schröter, M.; Ivanov, S. D.; Schulze, J.; Polyutov, S. P.; Yan, Y.; Pullerits, T.; Kühn, O., Exciton–vibrational coupling in the dynamics and spectroscopy of Frenkel excitons in molecular aggregates. *Physics Reports* **2015**, *567*, 1-78.
- (54) Ridley, J.; Zerner, M., An intermediate neglect of differential overlap technique for spectroscopy: Pyrrole and the azines. *Theoretica chimica acta* **1973**, *32* (2), 111-134.
- (55) Mallus, M. I.; Shakya, Y.; Prajapati, J. D.; Kleinekathöfer, U., Environmental effects on the dynamics in the light-harvesting complexes LH2 and LH3 based on molecular simulations. *Chemical Physics* **2018**, *515*, 141-151.
- (56) Olbrich, C.; Kleinekathöfer, U., Time-Dependent Atomistic View on the Electronic Relaxation in Light-Harvesting System II. *The Journal of Physical Chemistry B* **2010**, *114* (38), 12427-12437.
- (57) Olbrich, C.; Strümpfer, J.; Schulten, K.; Kleinekathöfer, U., Theory and Simulation of the Environmental Effects on FMO Electronic Transitions. *The Journal of Physical Chemistry Letters* **2011**, *2* (14), 1771-1776.
- (58) Nalbach, P.; Braun, D.; Thorwart, M., Exciton transfer dynamics and quantumness of energy transfer in the Fenna-Matthews-Olson complex. *Phys. Rev. E* **2011**, *84*, 041926.
- (59) Humphrey, W.; Dalke, A.; Schulten, K., VMD: Visual molecular dynamics. *Journal of Molecular Graphics* **1996,** *14* (1), 33-38.
- (60) Tong, A. L.; Fiebig, O. C.; Nairat, M.; Harris, D.; Giansily, M.; Chenu, A.; Sturgis, J. N.; Schlau-Cohen, G. S., Comparison of the Energy-Transfer Rates in Structural and Spectral Variants of the B800–850 Complex from Purple Bacteria. *The Journal of Physical Chemistry B* **2020**, *124* (8), 1460-1469.
- (61) Monshouwer, R.; Abrahamsson, M.; van Mourik, F.; van Grondelle, R., Superradiance and exciton delocalization in bacterial photosynthetic light-harvesting systems. *J. Phys. Chem. B* **1997**, *101*, 7241-7248.
- (62) Chachisvilis, M.; Kühn, O.; Pullerits, T.; Sundstrom, V., Excitons in photosynthetic purple bacteria: wavelike motion or incoherent hopping? *J. Phys. Chem.* **1997**, *101*, 7275-7283.
- (63) Georgakopoulou, S.; van Grondelle, R.; van der Zwan, G., Explaining the Visible and Near-Infrared Circular Dichroism Spectra of Light-Harvesting 1 Complexes from Purple Bacteria: A Modeling Study. *The Journal of Physical Chemistry B* **2006**, *110* (7), 3344-3353.
- (64) Novoderezhkin, V.; van Grondelle, R., Spectra and Dynamics in the B800 Antenna: Comparing Hierarchical Equations, Redfield and Förster Theories. *The Journal of Physical Chemistry B* **2013**, *117* (38), 11076-11090.
- (65) Bose, A.; Makri, N., All-mode quantum-classical path integral simulation of bacteriochlorophyll dimer exciton-vibration dynamics *J. Phys. Chem.* **2020**, *124*, 5028-5038.